Rendered and Characterized Closed-Loop Accuracy of Impedance-Type Haptic Displays

Nick Colonnese, *Student Member, IEEE*, Alexa F. Siu, *Student Member, IEEE*, Caroline M. Abbott, *Student Member, IEEE*, and Allison M. Okamura, *Fellow, IEEE*

Abstract—Impedance-type kinesthetic haptic displays aim to render arbitrary desired dynamics to a human operator using force feedback. To render realistic virtual environments, the difference between desired and rendered dynamics must be small. In this paper, we analyze the closed-loop dynamics of haptic displays for three common virtual environments: a spring, a damper, and a spring-damper, including the effects of time delay and low-pass filtering. Using a linear model, we identify important parameters for the rendered dynamics in terms of effective impedances, a conceptual tool that decomposes the displays closed-loop impedance into components with physical analogs. Our results establish bandwidth limits for rendering effective stiffness and damping. The effective stiffness bandwidth is limited by the virtual stiffness and device mass, and the effective damping bandwidth is limited by the cut-off frequency of the low-pass filter which filters the device velocity estimate. We show that a general system impedance can be characterized by a mass, damper, and spring optimally by the solution to a convex optimization problem, and we present a quantitative metric, the Average Distortion Error (ADE), to describe the fidelity of this model. Time delay has no significant effect on characterized stiffness, and reduces characterized damping by the product of virtual stiffness and total time delay. Reducing the low-pass filter cut-off frequency reduces the characterized damping. Experimental data gathered with a Phantom Premium 1.5 validates the theoretical analysis. We also conducted human user experiments to investigate the effects of time delay and low-pass filtering on perceived stiffness and damping. Similar to the characterized dynamics results, we observed no significant effect of time delay on perceived stiffness, and increasing time delay resulted in reduced perceived damping. Lower filter cut-off frequencies resulted in lower perceived damping. This work informs haptic display design by presenting how closed-loop behavior changes with key parameters.

Index Terms—Haptics, kinesthetic devices, transparency haptics system design and analysis

1 Introduction

Impedance-type kinesthetic haptic displays are composed of (1) a device equipped with sensors and actuators that provides force feedback to the user and (2) a rendering algorithm that computes force feedback as a function of device motion (Fig. 1).

Given a map from sensed position to actuator force (i.e., a virtual environment), the dynamics of the display are given by its closed-loop impedance, which describes the frequency-dependent relationship between input velocity (or position) and output force. The objective of accurate haptic rendering is to manipulate the rendered impedance of these displays to match a desired impedance through mechanical and feedback control design. Accurate haptic displays should feel exactly as desired, with no unwanted effects from a multitude of sources such as device dynamics (i.e., inherent inertia and friction), analog to digital (A/D) and digital to analog (D/A) conversions, aggressive low-pass filtering to mitigate noise, and amplifier or transport time delay. In addition to featuring the desired input-output characteristics, high-performance haptic displays must be stable and insensitive to noise. Past research has established rigorous conditions concerning stability and noise characterization. However, current results for haptic display accuracy are not complete. Describing the effect of system parameters (e.g., device damping and mass, and time delay) on the closed-loop properties would be a valuable tool in haptic display design. The analysis in this paper is about closed-loop display of stiffness and damping, two building blocks for rendering common desired dynamics.

1.1 Prior Work

This work builds on previous research on the accuracy of kinesthetic haptic displays and teleoperated systems. Analyzing the performance of a haptic display based on its input-output properties is similar to analyzing the "transparency" of a teleoperated system. For such systems, greater transparency translates to closer force and position signal matching between master and slave devices [19]. Christiansson and van der Helm analyzed the stability/transparency trade-off for bilateral teleoperation where the slave device had a built-in passive intrinsic stiffness [4]. Hirche et al. investigated how network-induced time delay affects the transparency of a teleoperator in terms of its mass, damping, and stiffness [16]. Although transparency is defined for teleoperator systems, not haptic displays, one can consider an analogy where the environment dynamics of a teleoperator are the desired dynamics of a haptic display, i.e., a perfectly transparent teleoperator would feature

- *N. Colonnese, C.M. Abbott, and A.M. Okamura are with the Department of Mechanical Engineering, Stanford University, Stanford, CA 94305. E-mail: {ncolonnese, cmabbott, aokamura}@stanford.edu.*
- *A.F. Siu is with the Department of Biomedical Engineering, Georgia Institute of Technology, Atlanta, GA 30332. E-mail: alexasiu@gatech.edu.*

Manuscript received 29 Oct. 2014; revised 18 June 2015; accepted 8 July 2015. Date of publication 17 July 2015; date of current version 11 Dec. 2015. Recommended for acceptance by K. Hashtrudi-Zaad.
For information on obtaining reprints of this article, please send e-mail to: reprints@ieee.org, and reference the Digital Object Identifier below.
Digital Object Identifier no. 10.1109/TOH.2015.2457438

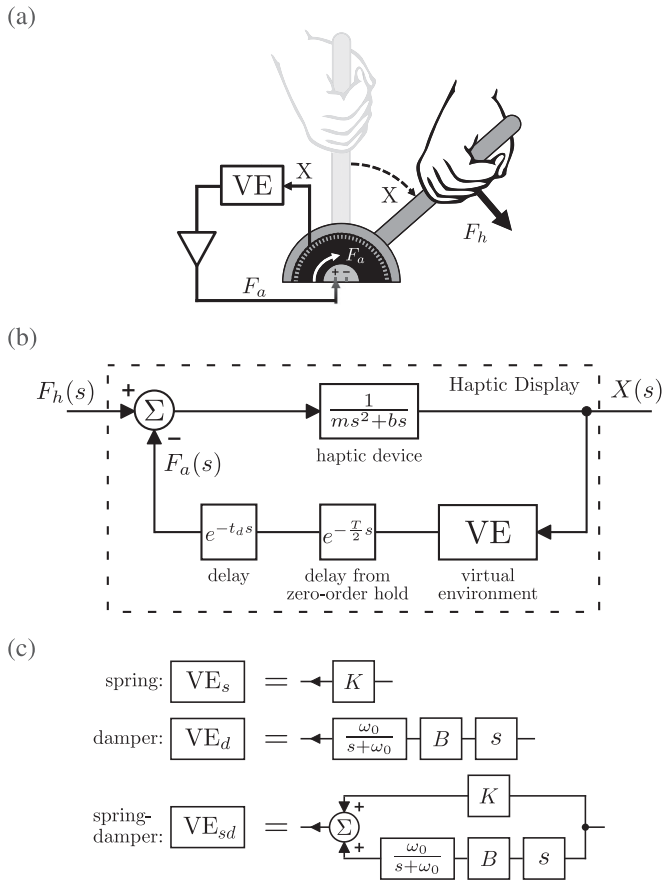

Fig. 1. (a) Schematic of a human interacting with an impedance-type (input position, output force) haptic device implementing a virtual environment. (b) Block diagram for this system. (c) The different types of virtual environments.

force feedback as if the user was interacting with the environment directly, and a perfectly accurate haptic display would feel exactly as desired.

Lawrence et al. experimentally explored accuracy in haptic displays by investigating the ability of humans to detect differences in impedances [20]. McJunkin et al. performed a similar experiment with a different scope by comparing the transparency bandwidth of a haptic display with both active (human input) and passive (motor driven) interaction tests [23]. In both of the studies, the experimental closed-loop behavior of the displays was analyzed. However, no theoretical models of how closed-loop behavior changes with system parameters were established.

Griffiths et al. defined a notion of accuracy for haptic displays called "distortion," which is similar to transparency [14]. Distortion is the frequency-dependent difference between actual and desired closed-loop dynamics, normalized by the desired dynamics. The concept is useful for elucidating abstract trade-offs in haptic design. However, because distortion does not analyze the closed-loop impedance directly, using it to identify the effect of system parameters can be difficult. No previous work has directly analyzed how distortion depends on time delay or low-pass filtering; both could affect the impedance of the display.

Colgate and Brown established conditions for robust stability of a haptic display coupled to a human operator in terms of haptic display passivity [5]. They defined Z-width: the range of virtual environment control law parameters that can be *commanded* resulting in a passive display. Because the commanded dynamics are generally different than the rendered dynamics, Z-width does not speak to haptic accuracy. In our analysis, we examine the accuracy of the rendered dynamics of the haptic display.

Extensive work has been performed on the effect of time delay on perceived stiffness using psychophysical experiments. Ishihara and Negishi, Knorlein et al., and Di Luca et al. reported that perceived stiffness *decreased* with time delay [17], [18], [22], and Pressman et al. reported that perceived stiffness *increased* with time delay [27]. Nisky et al. found that perceived stiffness depends on the nature of the haptic interaction [26]. These prior works examined how the *perceived* stiffness changed with time delay, and did not directly analyze how the actual mechanical properties of the haptic display change with time delay.

This paper expands upon our preliminary results [7]; here we present the rendered dynamics results from a new perspective, analyze the characterized dynamics, conduct experiments to validate the analysis, and perform human user experiments.

1.2 Contributions

In this paper, we address haptic accuracy by analyzing the closed-loop dynamics of haptic displays for three common virtual environments (VEs): a spring, a viscous damper, and a spring-damper. We include the effects of time delay and low-pass filtering. These environments are ubiquitous in practice for rendering "hard" surfaces, and are the building blocks for more complex virtual environments. For analyzing the closed-loop dynamics of a haptic display we consider different, but related, system descriptions.

Rendered Dynamics. The *rendered* dynamics describe the input-output properties of the closed-loop display using its mechanical impedance, $Z(s) = F(s)/V(s)$, where $V(s)$ is the input velocity, and $F(s)$ is the output force. A general (linear) system is fully described only by its rendered dynamics.

Characterized Dynamics. The *characterized* dynamics describe the system in terms of a finite number of simple parameters, e.g., mass, damping, and stiffness. The characterized dynamics cannot perfectly describe every haptic display, but provide a more simple description.

Perceived Dynamics. The *perceived* dynamics describe the haptic display using specific human user psychophysical experiments. Humans perceive the qualities of a haptic display not only as a function of the actual mechanical dynamics, and are influenced by visual information, the nature of physical exploration, semantics used in particular testing experiments, and other factors.

For the *rendered* dynamics, we analyze haptic accuracy by examining the closed-loop impedance of the haptic display including device dynamics, low-pass filtering, and time delay. We present the haptic display closed-loop impedance symbolically, and show it graphically using Bode and "effective impedances" plots. Mehling et al. first described effective damping and mass for a specific experimental impedance [24]. In our analysis, we expand the set of effective impedances to an infinite set of mechanical primitives (e.g., effective stiffness or effective jerk feedback), and

conduct a theoretical analysis examining the effective impedances of general haptic display, instead of a specific experimental one. Effective impedances present the same information as other frequency response tools, such as Bode or Nyquist plots, but express the system response through physical analogs. Our results, given in terms of effective impedances, demonstrate that spring and spring-damper haptic displays render a nonzero effective stiffness for frequencies only up to $\omega_s^* = \sqrt{K/m}$, where K represents the virtual stiffness, and m the device mass. Damper and spring-damper displays render the desired effective damping for frequencies up to the cut-off frequency of the low-pass filter ω_0. Time delay reduces the effective damping of spring and spring-damper displays, reduces the effective mass for pure damper displays, and can introduce energy generating "effective jerk feedback," which can be interpreted of as negative damping. Concrete takeaways for the design of haptic displays are presented in Section 7. We validate the theoretical results by constructing experimental frequency responses using a Phantom Premium 1.5 haptic device in Section 6.1.

For the *characterized* dynamics, we show that an "optimal" mass, damper, and spring model of general system impedance can be formed by the solution to a convex optimization problem. The fidelity of this model is provided by a quantitative metric, the Average Distortion Error (ADE). We analyze the classic spring-damper closed-loop rendering and show that time delay has no significant effect on characterized stiffness, but reduces characterized damping by the product of virtual stiffness and total time delay. We also show that for lower low-pass filter cut-off frequencies, corresponding to more aggressive filtering, the lower the characterized damping. We validate the theoretical predictions for the characterized dynamics by conducting time-based system identifications on experimental data in Section 6.2.

For the *perceived* dynamics, we perform human user experiments that reveal how low-pass cut-off frequency and time delay affect perceived stiffness and damping. The perceived results are similar to the characterized dynamics results: we observed no significant effect of time delay on perceived stiffness, and increasing time delay resulted in reduced perceived damping. Lower cut-off frequencies resulted in lower perceived damping.

This work informs the design of haptic displays by modeling how the closed-loop system is affected by haptic device dynamics, time delay, and low-pass filtering. By understanding the actual mechanical dynamics of the display, and demonstrating the influence of those dynamics on human perception, we form a foundation for future work to rigorously analyze human perception of haptic qualities.

2 System Models

Here we introduce system models for a human interacting with a 1-degree-of-freedom (1-dof) impedance-type haptic device rendering virtual environments. The system models are used to generate theoretical closed-loop impedances for haptic displays. The system models are similar to prior work analyzing the stability and accuracy of haptic displays [1], [8], [12], [14].

Fig. 1 gives a schematic and block diagram for the system model. The haptic device is modeled as a mass m with viscous damping b. We analyze three virtual environments, that map sensed position to actuator forces: a spring, a damper, and a spring-damper consisting of a spring and damper in parallel. These virtual environments were chosen for their ubiquity in rendering "hard" dynamics in practice (e.g., a virtual wall), as well as for their simplicity. The damper feedback requires a differentiation of sensed position. Because differentiation amplifies high-frequency noise, the velocity estimate is low-pass filtered with a unity gain filter at zero frequency and a cut-off frequency of ω_0 (rad/s). Linear, continuous models are used for the straightforward application of frequency response tools. To account for the fact that control is performed through a computer containing A/D and D/A components, a time delay of half the sample time is included in the feedback loop. In addition to this inherent system delay, there is also an external time delay t_d resulting from potential amplifier or transport delay.

For systems that are not well described by our model, e.g., haptic displays with large device friction or slow sampling rates, the parameters may affect accuracy differently.

3 Effective Impedances

In this section we present a decomposition of a system impedance into "effective impedances." Effective impedances aim to aid the interpretation of a haptic display impedance as "mechanical primitives" such as mass, damping, and stiffness.

For a transfer function representing the impedance of a system, $Z(s) = F(s)/V(s)$, the effective impedances are defined as

$$\begin{aligned}
&\vdots \\
\text{Eff. Integral FB} &= EIF(\omega) = \omega^2 \mathfrak{Re}^-\{Z(j\omega)\} && -270^\circ \le \theta \le -90^\circ, \\
\text{Eff. Stiffness} &= ES(\omega) = \omega \mathfrak{Im}^-\{Z(j\omega)\} && -180^\circ \le \theta \le 0^\circ, \\
\text{Eff. Damping} &= ED(\omega) = \mathfrak{Re}^+\{Z(j\omega)\} && -90^\circ \le \theta \le 90^\circ, \\
\text{Eff. Mass} &= EM(\omega) = \omega^{-1} \mathfrak{Im}^+\{Z(j\omega)\} && 0^\circ \le \theta \le 180^\circ, \\
\text{Eff. JerkFB} &= EJF(\omega) = \omega^{-2} \mathfrak{Re}^-\{Z(j\omega)\} && 90^\circ \le \theta \le 270^\circ, \\
&\vdots
\end{aligned}$$

where FB is an abbreviation for feedback and $\theta = \angle Z(j\omega)$. The dots show that effective impedances are defined for any $\angle Z(j\omega)$.

Effective impedances decompose the system impedance into components that coincide with physical analogs. For example, effective stiffness is the component of the force in phase with position. Some effective impedances, e.g., jerk and higher derivatives of position feedback, do not have simple mechanical analogs. Fig. 2 shows a chart of the phase of $Z(j\omega)$ and its effective impedances for real and imaginary components.

When the system impedance is displayed using a Nyquist plot, the effective impedances are the projections onto the real or imaginary axes, normalized by the appropriate power of frequency. E.g., effective damping is the projection onto the real axis (for $-90^\circ \le \angle Z(j\omega) \le 90^\circ$).

4 Closed-Loop System Analysis

In this section we analyze the closed-loop dynamics of haptic displays with and without time delay for spring, viscous damper, and spring-damper virtual environments. For a

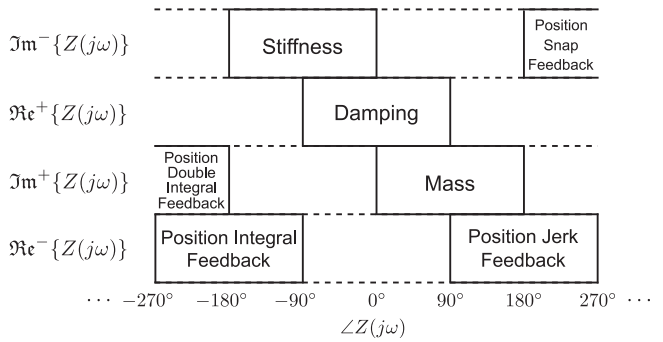

Fig. 2. Effective impedances are defined for both signs of the real and imaginary components of $Z(j\omega)$, and its angle $\angle Z(j\omega)$. Those defined by the real component are energy generating or dissipating, and those defined by the imaginary component neither generate nor dissipate energy.

given virtual environment, VE, the display's closed-loop impedance is

$$\frac{F_h(s)}{V(s)} = Z(s) = \frac{1 + G_d[\mathrm{VE}e^{-j\omega(T/2+t_d)}]}{G_d s}, \tag{1}$$

where G_d represents the position to force transfer function of the haptic device,

$$G_d = \frac{1}{ms^2 + bs}, \tag{2}$$

T is the sample period, and t_d is the external delay. The mass and damping of the haptic device used to generate Figs. 3, 4, 5 are $m = 100$ (g), and $b = 0.1$ (Ns/m).These values were chosen to be representative of existing impedance-type haptic devices [8]. Our analysis will identify symbolic expressions for (1) the effective stiffness bandwidth, $\sqrt{K/m}$; (2) the effective damping bandwidth, ω_0; (3) the relationship between reduction in effective damping and time delay, $-K(T/2 + t_d)$; and (4) the relationship between reduction in effective mass and time delay, $-B(T/2 + t_d)$.

4.1 Spring

The closed-loop impedance of a haptic display rendering a *spring* is

$$Z_s(s) = \frac{ms^2 + bs + Ke^{-j\omega(T/2+t_d)}}{s}. \tag{3}$$

The Bode and effective impedance plots for this system are shown in Fig. 3 with varying values for the total time delay.

For parameter values in which the system is stable [12], its frequency response has a magnitude close to K/ω and a phase of $-90°$ up to a critical frequency,

$$\omega_s^* = \sqrt{\frac{K}{m}}. \tag{4}$$

The resonance peak at ω_s^* and frequency span for which the phase of the system changes depends on device damping *and* the total time delay. For frequencies less than ω_s^*, the display has effective stiffness, ES, of K, and effective mass, EM, of zero. For frequencies larger than ω_s^*, ES is zero, and

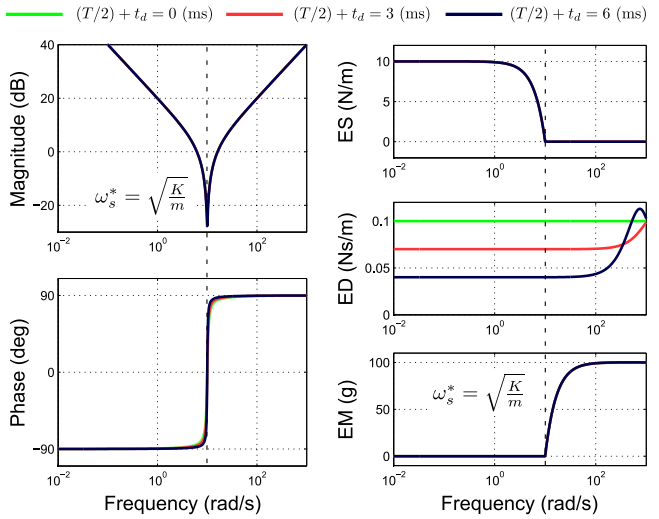

Fig. 3. Spring VE Bode and effective impedance plots with $K = 10$ (N/m) and varying amounts of total delay. The displays have an ES close to K up to the effective stiffness bandwidth at $\omega_s^* = \sqrt{K/m}$, after which, ES drops to zero and EM dominates. Delay reduces ED by $K(T/2 + t_d)$, but does not significantly affect ES or EM.

EM tends to the device mass. The desired dynamics of a spring haptic display is a constant stiffness across all frequencies. Adding delay to the system *decreases* ED by $K(T/2 + t_d)$ for lower frequencies.

4.2 Viscous Damper

The closed-loop impedance of a haptic display rendering a *damper* is

$$Z_d(s) = \frac{ms^2 + (m\omega_0 + b)s + (b + Be^{-j\omega(T/2+t_d)})\omega_0}{s + \omega_0}. \tag{5}$$

System behavior depends on how the cut-off frequency of the low-pass filter, ω_0, compares to $\bar{\omega} = (b + B)/m$, which represents a pole of the damper display with no low-pass filter.

The Bode and effective impedance plots of the damper closed-loop displays are shown in Fig. 4 with varying values for the low-pass filter cut-off frequency, ω_0, and total time delay, $(T/2\tilde{} + \tilde{}t_d)$. For varying cut-off frequency, we consider three conditions: (1) $\omega_0 \ll \bar{\omega}$, (2) $\omega_0 \approx \bar{\omega}$, and (3) $\omega_0 \gg \bar{\omega}$.

For no delay, when the system is stable, the ED is the sum of the device and virtual damping, $(b + B)$, for frequencies less than ω_0, and just the device damping, b, for higher frequencies.

Adding delay to the system affects its closed-loop impedance in two ways. First, delay reduces EM from the no-delay value by $B(T/2 + t_d)$. This is similar to delay reducing ED in the spring environment by $K(T/2 + t_d)$. Second, delay reduces ED bandwidth, and introduces oscillations in ED for frequencies past ω_0. These oscillations can introduce nonzero energy generating effective jerk feedback, EJF, at higher frequencies.

4.3 Spring-Damper

The closed-loop impedance of a haptic display rendering a *spring-damper* is

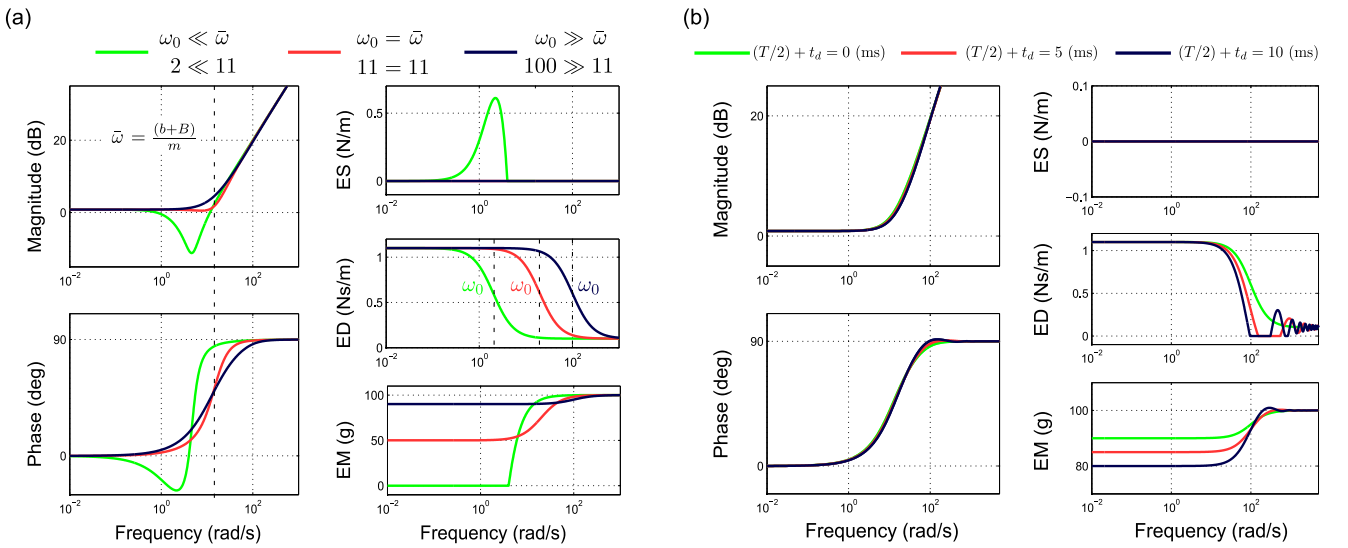

Fig. 4. Damper VE Bode and effective impedance plots with $B = 1$ (Ns/m) for (a) varying low-pass filter cut-off frequency, and (b) varying total time delay for $\omega_0 \gg \bar{\omega} = (b + B)/m$. (a) The effective damping bandwidth is ω_0. The colored ω_0 represents the distinct cut-off frequencies for the three systems. As ω_0 is reduced, corresponding to more aggressive filtering, EM and the ED bandwidth are reduced. When $\omega_0 < \bar{\omega} = (b + B)/m$, the system has nonzero ES. (b) Increasing delay reduces the ED bandwidth. EM is reduced by $B(T/2 + t_d)$ from its no-delay value at low frequencies.

$$Z_{sd}(s) = \frac{ms^3 + (m\omega_0 + b)s^2 + [b\omega_0 + (B\omega_0 + K)d]s + K\omega_0 d}{s(s + \omega_0)}, \tag{6}$$

where

$$d = e^{-j\omega(T/2+t_d)}. \tag{7}$$

The Bode and effective impedance plots of the spring-damper displays are shown in Fig. 5 with varying values for the low-pass filter cut-off frequency, ω_0, and total time delay, $(T/2 + t_d)$.

Like the pure spring display, the magnitude of the frequency response is close to K/ω and the phase is -90° for frequencies less than ω_s^*. The resonance peak at ω_s^* and frequency span for which the phase of the system changes from -90° to 90° depends on the *effective* damping (in contrast to the device damping as was the case for the spring environment) and total time delay. For frequencies less than ω_s^*, the display has an ES of K, and an EM of zero. For frequencies larger than ω_s^*, ES is zero, and EM tends to the device mass. The ED is the sum of the device and virtual damping, $(b + B)$, for frequencies less than ω_0, and just the device damping, b, for frequencies larger. These results establish that the spring-damper display has an ES bandwidth given by Equation (4), and an ED bandwidth of the cut-off frequency ω_0.

Delay affects the spring-damper display much like it does for the pure spring and damper environments. Adding delay reduces ED by $K(T/2 + t_d)$ for frequencies less than ω_0 and

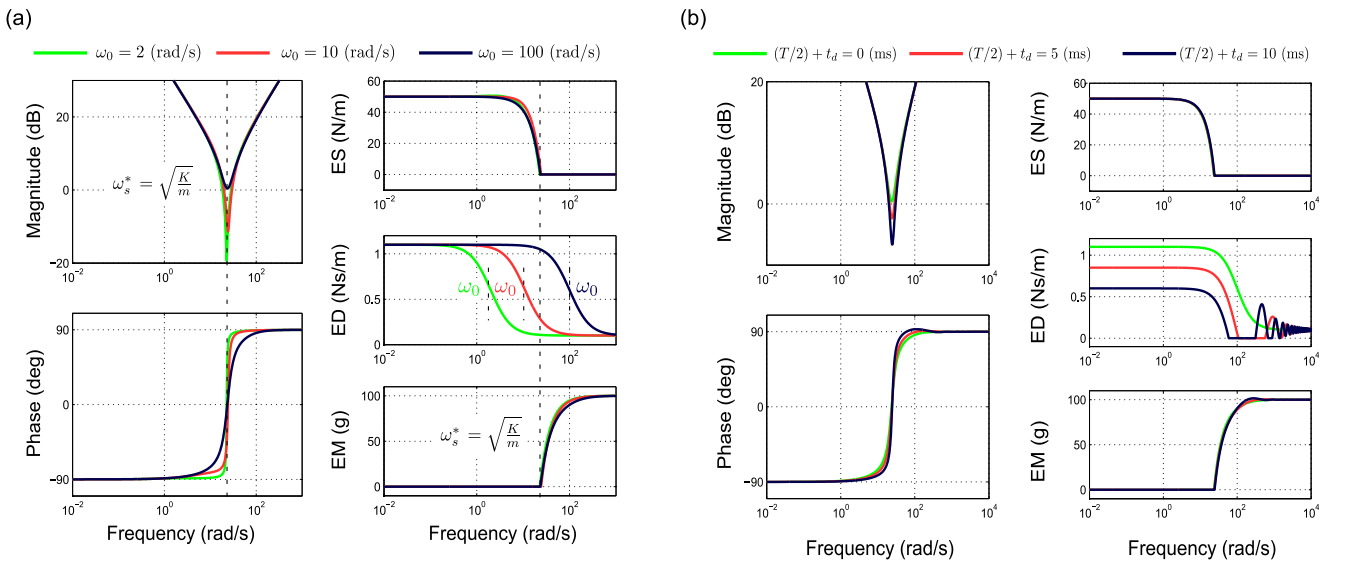

Fig. 5. Spring-damper VE Bode and effective impedance plots with $K = 50$ (N/m), $B = 1$ (Ns/m), for (a) varying low-pass filter cut-off frequency, and (b) varying total time delay. The systems have an ES of K up to $\omega_s^* = \sqrt{K/m}$, after which the ES drops to zero and the EM dominates. (a) As ω_0 is reduced, so is the frequency span for which the ED is $(b + B)$. (b) Time delay reduces the ED by $K(T/2 + t_d)$ at low frequencies, but does not significantly affect the ES or EM.

also introduces oscillations in ED (which can introduce nonzero EJF at some frequencies), for frequencies past ω_0.

5 Characterizing a General Impedance as a Mass, Damper, Spring

In this section we form a mass, damper, spring model that characterizes the dynamics of a system by solving a convex optimization problem, which is formulated by minimizing an objective function called the "Average Distortion Error:" a quantitative scalar metric describing the similarity of two impedances.

5.1 Average Distortion Error

Griffiths et al. defined haptic distortion, the frequency-dependent difference between actual and desired closed-loop dynamics, normalized by the desired dynamics [14]. Distortion is an infinite dimensional metric for the accuracy of a haptic display. Here we define the Average Distortion Error, which is a scalar quantity describing haptic accuracy:

$$\mathrm{ADE} = \frac{1}{(\omega_2 - \omega_1)} \int_{\omega_1}^{\omega_2} W(\omega) \left| \frac{Z(j\omega) - Z_d(j\omega)}{Z_d(j\omega)} \right| d\omega, \quad (8)$$

where $W(\omega)$ is the weighting function, and the frequencies ω_1 and ω_2, where $\omega_2 \geq \omega_1$, define the considered frequencies. The weighting function is included to examine the sensitivity of the optimized parameters with respect to various weightings. In our analysis, we consider linear and logarithmic weighting functions.

5.2 Forming a Mass, Damper, Spring Model of a General System Impedance

The parameters of a mass, damper, spring model, $Z_{MBK}(s)$, of system impedance, $Z_{sys}(s)$, are formed by the solution to

$$\min_{\hat{M},\hat{B},\hat{K}} \int_{\omega_1}^{\omega_2} W(\omega) \left| \frac{Z_{MBK}(j\omega) - Z_{sys}(j\omega)}{Z_{sys}(j\omega)} \right| d\omega \quad (9)$$

$$\text{subject to } \hat{M}, \hat{B}, \hat{K} \geq 0, \quad (10)$$

where $\hat{M}$, $\hat{B}$, $\hat{K}$, are the mass, viscous damping, and stiffness of the model, respectively,

$$Z_{MBK} = \hat{M}(j\omega) + \hat{B} + \frac{\hat{K}}{(j\omega)}. \quad (11)$$

The optimization variables $\hat{M}, \hat{B}, \hat{K}$ are convex (affine) in the objective function, and the feasible region is a convex set. Because of this, the global solution to optimization (9) can be found efficiently [2]. In our analysis, we used CVX, a package for solving convex programs [13]. The physical interpretation of optimization (9) is that a mass, damper, spring model of a system can be formed by choosing the parameters of the model that minimize ADE over a large range of frequencies.

5.3 Function of Interaction Frequencies

In this section we show that the accuracy of the mass, damper, spring model for a general haptic display is a function on the frequencies of interaction.

5.3.1 Single Interaction Frequency

If a general impedance is excited at a single frequency, the mass, damper, spring model is exact. On other words, it is possible to choose mass, damping, and stiffness parameters such that the input-output properties of *any* system impedance match the input-output properties of the mass, damper, spring impedance.

To see this, consider a system impedance, $Z_{sys}(s)$, excited at frequency ω_1. The input-output properties of the system are described by its real and imaginary components

$$Z_{sys}(j\omega_1) = \frac{F(j\omega_1)}{V(j\omega_1)} = x + jy. \quad (12)$$

For the mass, damper, spring system, $Z_{MBK}(s)$, to have the same input-output properties at the same frequency we require

$$Z_{sys}(j\omega_1) = Z_{MBK}(j\omega_1). \quad (13)$$

This occurs if

$$x + jy = m(j\omega_1) + B + \frac{K}{(j\omega_1)}, \quad (14)$$

which implies

$$x = B, \quad (15)$$

$$y = m\omega_1 - \frac{K}{\omega_1}. \quad (16)$$

Because Equation (14) has three variables, but only two equations, there exists a *set* of mass, damper, spring impedances that have precisely the same input-output properties as the system.

5.3.2 Many Interaction Frequencies

If an impedance is excited with *many* interaction frequencies, the mass, damper, spring model will in general not have the same input-output properties. The difference between the system and model behavior depends on the frequencies considered.

To see this, we consider the system impedance's input-output properties at each frequency of excitation

$$Z_{sys}(j\omega_i) = \frac{F(j\omega_i)}{V(j\omega_i)} = x_i + jy_i \qquad \text{for } i = 1, \ldots, n, \quad (17)$$

where n represents the number of frequencies. For $Z_{MBK}(s)$ to have the same input-output properties we require

$$Z_{sys}(j\omega_i) = Z_{MBK}(j\omega_i) \qquad \text{for } i = 1, \ldots, n. \quad (18)$$

This occurs if

$$x_i + jy_i = m(j\omega_i) + B + \frac{K}{(j\omega_i)} \qquad \text{for } i = 1, \ldots, n, \quad (19)$$

which in general, cannot be satisfied. This means that a mass, damper, spring model cannot describe every impedance exactly at all frequencies. The disparity between the system and model is described by the Average Distortion Error: the larger the ADE, the larger the disparity.

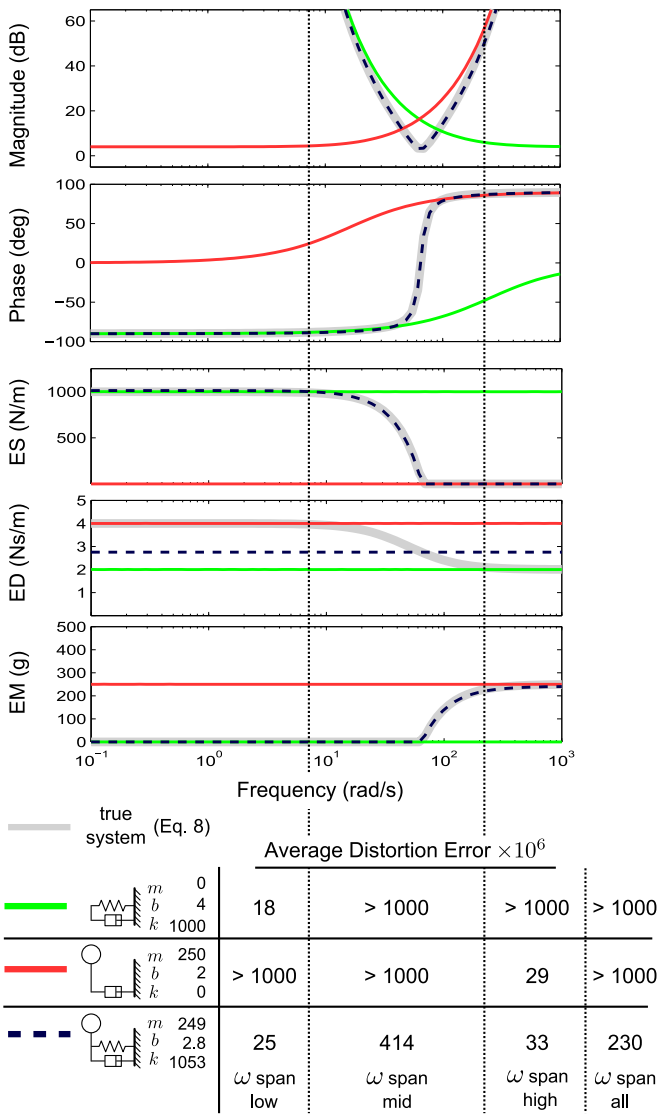

Fig. 6. Bode and effective impedance plots of the closed-loop spring-damper impedance (Equation (6)), various mass, damper, spring model impedances, and the corresponding average distortion errors over different frequency ranges. The optimal model formed using optimization (9) has the lowest ADE over the entire frequency range.

5.4 Example: Mass, Damper, Spring Models of Closed-Loop Spring-Damper Rendering

Here we present an example comparing a classic closed-loop spring-damper haptic rendering including the effects of the haptic device dynamics, time delay, and low-pass filtering (Equation (6)), to various mass, damper, spring impedances to highlight different system behavior over different frequency ranges.

Fig. 6 shows the Bode and effective impedance plots of the closed-loop spring-damper rendering and three different mass, damper, spring impedances. For each model, we calculate the ADE between the model and the closed-loop virtual spring and damper rendering (Equation (6)), for four different frequency ranges: low, $0.1-7$, medium, $7-210$, high, $210-1000$, and all, $0.1-1000$ (rad/s). The particular frequency spans were chosen to highlight different true system behavior at different frequencies, i.e., the frequency spans were chosen relating to the effective stiffness and damping bandwidths of Equation (6).

TABLE 1
Optimal $\hat{M}, \hat{B}$, and $\hat{K}$ for Weighting Functions

$W(\omega)$	$\hat{M}$ (g)	$\hat{B}$ (Ns/m)	$\hat{K}$ (N/m)
linear	249	2.79	1,053
logarithmic	249	2.85	1,058

One model has damping and stiffness, but no mass. Another model has mass and damping, but no stiffness. The last model is formed using optimization (9) and has mass, damping, and stiffness. To test the sensitivity of the optimal solutions (i.e., the characterized mass, damping and stiffness), of optimization (9) with respect to the weighting function, we calculated the solutions using two different weighting functions: linear, $W(\omega) = 1$, and logarithmic, $W(\omega) = \log(\omega)$. The solutions are shown in Table 1. Our analysis shows that the solutions are insensitive to the weighting function, i.e, the optimal characterized mass, damping, and stiffness are not significantly different.

At low frequencies, the models with damping and stiffness have similar dynamics to the closed-loop spring-damper rendering, Equation (6), but the dynamics of the model with no stiffness are vastly different. This is because the majority of the force of the system impedance comes from the stiffness component.

At high frequencies, the models with damping and mass have similar dynamics to the closed-loop spring-damper rendering, Equation (6), but the dynamics of the model with no mass are different. Here, the majority of the force of comes from the mass.

For the medium frequencies, near the effective stiffness bandwidth of the display, Equation (4), the model fit using optimization (9) with mass, damping, and stiffness, has a significantly smaller ADE than the other models. At these frequencies, the system impedance requires mass, damping, and stiffness components to adequately describe the dynamics.

6 Experimental Validation

In this section we present the experimental rendered, characterized, and perceived dynamics. First, we show the closed-loop rendered impedances, or experimental transfer function estimates, of the spring-damper virtual environment haptic displays to compare experimental data to the theoretical predictions in Section 4. Then, we analyze how time delay and low-pass filtering affect the characterized and perceived stiffness and damping of a closed-loop haptic display using time-based system identifications. The experimental characterizations are compared to theoretical predictions formed using the optimization procedure described by optimization problem (9) in Section 5. Finally, we experimentally determine the perceived stiffness and damping by performing a human user study.

Experiments were conducted on a single joint (the first revolute joint) of a Phantom Premium 1.5. The other degrees of freedom were mechanically constrained by a custom-made fixture.

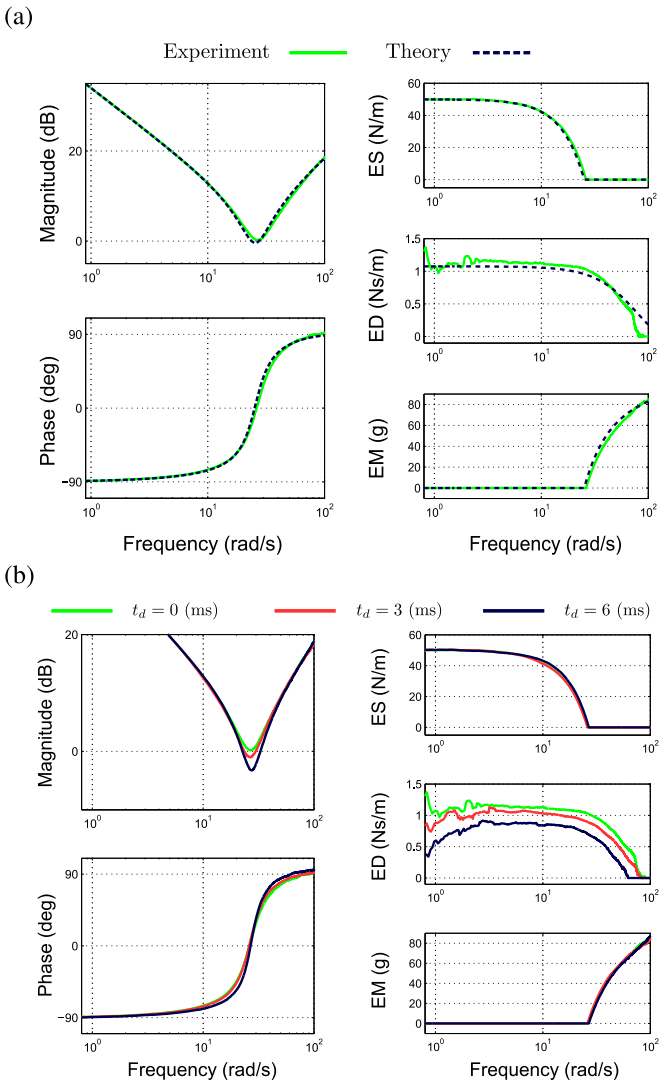

Fig. 7. Experimental Bode and effective impedance plots for the closed-loop spring-damper display with (a) no external time delay, and (b) external time delay. (a) The experimental data are similar to theoretical predictions. (b) As predicted from theory (see Fig. 5b), delay reduces ED by $K(T/2 + t_d)$ from its no-delay value, but does not affect ES or EM.

6.1 Rendered Dynamics Experiments

To verify the theoretical predictions, we experimentally determined the frequency response of the closed-loop spring-damper haptic display with and without time delay. The parameters of the haptic display were $K = 50$ (N/m), $B = 1$ (Ns/m), and $\omega_0 = 125$ (rad/s). The external delay was implemented in software in multiples of the sample time. For each experiment, an exogenous white noise input force excited the system for two minutes at a sample rate of 1 kHz. Raw impedances were computed by the ratio of the discrete Fourier transform of the system's force and position [21]. The raw impedances were smoothed in the complex domain using a Hamming window with a length of 200 points. The experimental effective impedances were formed by the equations presented in Section 3. The theoretical results for comparison use the device parameters found in Section 6.2.

Fig. 7 displays the experimental Bode and effective impedance plots of the spring-damper display with and without added external delay. For no added external delay, Fig. 7a, the experimental results are similar to theoretical predictions: ES is 50 (N/m) for frequencies up to $\omega_s^* = 23$ (rad/s), after which it drops to zero. ED is close to the predicted value of $(b + B)$ for low frequencies, and drops near $\omega_0 = 125$ (rad/s). EM is zero up to ω_s^*, and tends to the device mass as frequency increases. The experimental data for the spring-damper display with added external delay, Fig. 7b, can be compared to Fig. 5b, which displays the corresponding theoretical results. As predicted by theory, larger delay in the control loop corresponds to a larger magnitude resonance peak at ω_s^* in the Bode plot. Time delay reduces the ED by approximately $K(T/2 + t_d)$ from its no-delay value, but does not significantly affect the ES or EM. It was difficult to produce experimental data that were not corrupted by noise for very low and very high frequencies. Because of this, we were unable to observe experimental data at the frequencies where effective damping scillations were predicted to occur.

6.2 Characterized Dynamics: System Identification of Open and Closed-Loop Haptic Display Properties

A time-based system identification procedure was used to determine the open-loop properties of the Phantom Premium 1.5, and the closed-loop properties of the haptic display with various amounts of time delay and low-pass filtering.

Ideally, at every instant in time the system should satisfy

$$f(t) = \hat{m}\ddot{x}(t) + \hat{b}\dot{x}(t) + \hat{k}x(t), \tag{20}$$

where $f(t)$ is the external force, $\ddot{x}(t)$, $\dot{x}(t)$, and $x(t)$ are the acceleration, velocity, and position of the device, respectively, and $\hat{m}$, $\hat{b}$, and $\hat{k}$ represent the mass, damping, and stiffness of the system, respectively. For a particular experiment, the system was excited with an exogenous chirp force using the motor of the Premium 1.5 from 0.1 to 25 Hz, and its position was measured. Velocity and acceleration signals were generated by numerical differentiation and smoothed with non-causal low-pass filters with no phase lag. Parameters $\hat{m}$, $\hat{b}$, and $\hat{k}$ were computed from the experimental data via optimization,

$$\hat{m}, \hat{b}, \hat{k} = \text{argmin} \sum (f_i - \hat{m}\ddot{x}_i - \hat{b}\dot{x}_i - \hat{k}x_i)^2, \tag{21}$$

where f_i, $\ddot{x}_i$, $\dot{x}_i$, x_i represent the signal values at a specific instants. The pseudo-inverse was used to solve optimization (21) [29].

The Phantom Premium 1.5 open-loop parameters averaged over five experiments were: $\hat{m} = 94, \sigma_{\hat{m}} = 4$ (g), $\hat{b} = 0.10, \sigma_{\hat{b}} = 0.02$ (Ns/m), and $\hat{k} < 1, \sigma_{\hat{k}} = 1$ (N/m), where σ represents the standard deviation of an estimate. These values are similar to those reported in [3] and [8].

Fig. 8 displays the experimental and theoretical closed-loop haptic display stiffness and damping characterizations. The time-based system identification experimental data are similar to the theoretical characterizations performed using optimization (9).

6.3 Perceived Dynamics: Human User Experiments

A user study based on the psychophysics method of adjustments was conducted to investigate the effect of time delay and low-pass filtering on perceived stiffness and damping.

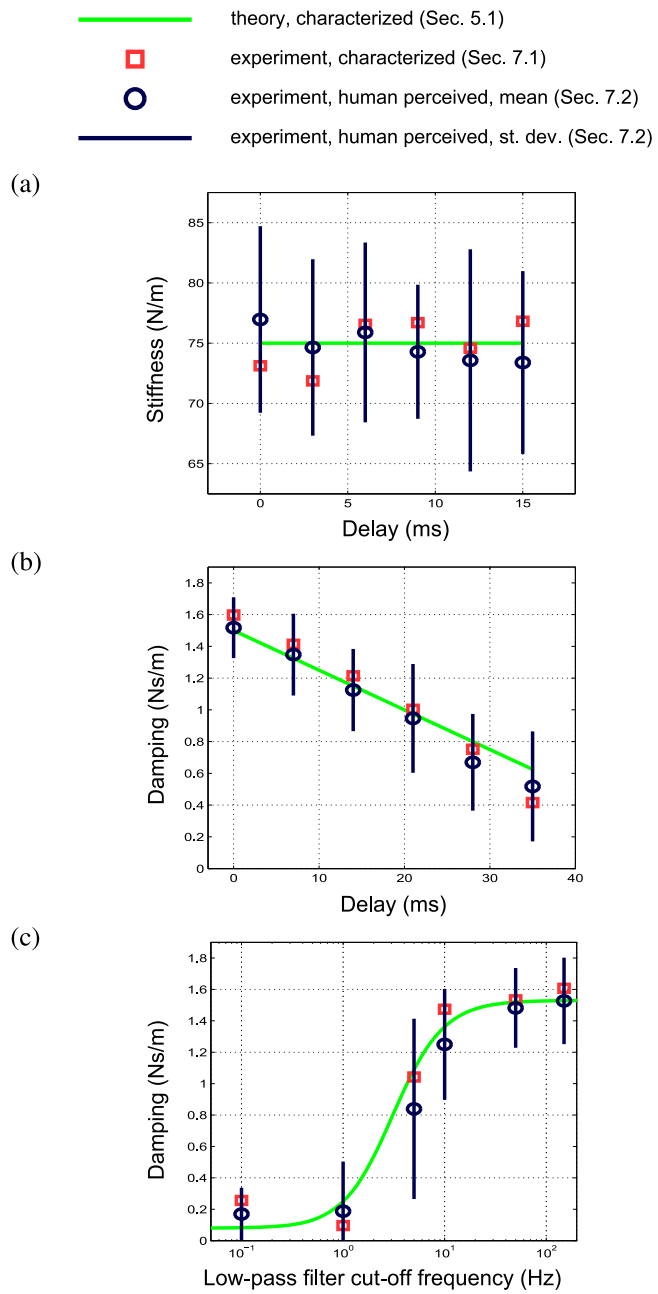

Fig. 8. Theoretical characterizations Section (5.2), experimental system identification characterizations Section (6.2), and experimental human user perceived dynamics Section (6.3), for: (a) effect of delay on stiffness, (b) effect of delay on damping, and (c) effect of low-pass filter cut-off frequency on damping. The experimental system identification and human user data are similar to theoretical characterizations. Time delay has no significant effect on stiffness, but *reduces* damping by the product of virtual stiffness and total time delay. The low-pass filter cut-off frequency affects damping strongly: for low cut-off frequencies, the damping is approximately the natural damping of the haptic display, for high cut-off frequencies, the damping is approximately the sum of the natural and virtual damping.

6.3.1 Participants

A total of 16 participants (eight males and eight females) between the ages of 19 and 50 (with a mean age of 25) participated in the experiment. Fifteen are right handed. The experiment protocol was approved by the Stanford Institutional Review Board.

6.3.2 Task

The experiments investigated the effect of delay and low-pass filtering on the user's perception of stiffness and damping using the method of adjustments [11]. Three different cases were presented to the users: (1) effect of time delay on perceived stiffness, (2) effect of time delay on perceived damping, and (3) effect of low-pass filter cut-off frequency on perceived damping. The independent parameters were time delay and low-pass filter cut-off frequency, and the dependent parameters were the perceived stiffness and damping.

In the tasks, users manipulated the stiffness or damping of a "tunable" virtual environment (with no added time delay, and a very high low-pass filter cut-off frequency), until they were satisfied by the equality of the tunable virtual environment to another virtual environment, potentially with non-zero time delay, or a much lower low-pass filter cut-off frequency. The experiments were designed to test the actual mechanical properties as closely as possible: we provided no visual avatar of the device position, and did not enforce a particular probing strategy.

The experiments to test the effect of time delay on perceived stiffness used time delays of 0, 3, 6, 9, 12, and 15 ms. The base case had a stiffness of 75 N/m, a damping of 2 Ns/m, a cut-off frequency of 150 Hz, and no delay. The tunable case began at 5 or 150 N/m, and could be adjusted in increments of 5 N/m. The Weber fraction for stiffness is 0.039 [15].

The experiments to test the effect of time delay on perceived damping used time delays of 0, 7, 14, 21, 28, and 35 ms. The effect of low-pass filter cut-off frequency on perceived damping experiments tested cut-off frequencies of 0.1, 1, 5, 10, 50, and 150 Hz. The base case for both experiments on perceived damping had a stiffness of 25 N/m, a damping of 1.5 Ns/m, a cut-off frequency of 150 Hz, and no delay. The tunable case began at 0 or 3 Ns/m, and could be adjusted in increments of 0.25 Ns/m. The Weber fraction for damping is 0.147 [25].

The tested time delays and low-pass filter cut-off frequencies were chosen to be representative of typical current-day haptic displays [8], [14]. Different sets of time delay values were chosen for the stiffness and damping experiments to span the largest range such that the haptic displays were uncoupled stable [12]. This was done for practical reasons, because the characterized experiments (Section 6.2), were done with the same set of parameters, and were performed with no human.

For a particular time delay or cut-off frequency, the tunable case started at the low extreme for one trial, and the high extreme for the other. In each set of experiments, the order of the tested time delays or cut-off frequencies was randomized.

6.3.3 Procedure

The experiments were conducted on a single degree of freedom (dof) of the Phantom Premium 1.5 haptic device. Users were instructed to use their dominant hand to grasp the Phantom arm for all experiments, and were given five minutes before the experiments to explore a sample virtual environment and learn the format of the trials. Each user performed two trials for each tested time delay or cut-off

TABLE 2
Statistics for Perceived Dynamics Experimental Data

	ANOVA p value	regression model	regression model parameter fits and 95% confidence intervals	regression r^2
Effect of delay on perceived stiffness	0.45	linear $\hat{K} = \alpha t_d + K_0$	α: -0.22 [-0.44 0.00]; K_0: 76.4 [74.4 78.4]	0.02
Effect of delay on perceived damping	< 0.001	linear $\hat{B} = \beta t_d + B_0$	β: -0.03 [-0.02 -0.04]; B_0: 1.53 [1.45 1.61]	0.61
Effect of low-pass cut-off frequency on perceived damping	< 0.001	sigmoid $\hat{B} = B_{\mathrm{low}f} + \frac{B_{\mathrm{low}f} - B_{\mathrm{high}f}}{1+10\hat{}\{(\bar{f}-f_0)B_{slope}\}}$	$B_{\mathrm{low}f}$: 0.11 [0.02 0.20]; $B_{\mathrm{high}f}$: 1.50 [1.41 1.59]; $\bar{f}$: 2.55 [-3.75 8.86]; B_{slope}: 0.12 [0.04 0.20]	0.57

Stiffness is in units of N/m, damping in Ns/m, time delay in s, and frequency in Hz. The brackets represent the 95 percent confidence interval for the for the regression parameters.

frequency, for three experiment cases, for a total of $2 \times 6 \times 3 = 36$ trials. The users had a mandatory two minute break in between each of the experiments, and the mean time for all experiments was 30 minutes.

6.3.4 Results

The results are shown in Fig. 8, and the statistics for the perceived dynamics are shown in Table 2. The experimental data show the averages over all participants, and the standard deviations. The human user experiment data are similar to the time-based system identification experiment data, as well as the theoretical characterization predictions. Time delay had no significant effect on perceived stiffness ($p = 0.45$), but reduced perceived damping by approximately the product of virtual stiffness and total time delay ($p < 0.001$). The lower the value of the low-pass filter cut-off frequency, corresponding to more aggressive filtering, the lower the perceived damping ($p < 0.001$).

7 Discussion

Our results demonstrate a fundamental relationship between the system parameters given by Equation (4) and the frequency span over which the spring and spring-damper displays render an effective stiffness. This relationship informs the design of spring-type displays intending to render a stiffness. Specifically, for high effective stiffness bandwidth, large virtual spring constants and low device mass are desired. Large spring constants are usually desired, but are constrained by the stability of the display [12]. The mass of most haptic devices is as small as practical to reduce open-loop inertia. Although these design objectives match conventional design, most spring-type haptic displays (with mass greater than 100 g, and maximum virtual stiffness less than 400 N/m) are necessarily low bandwidth (less than 10 Hz).

Unlike the effective stiffness bandwidth, the bandwidth of effective damping feedback in haptic displays is limited by the cut-off frequency of the low-pass filter. For many haptic displays, virtual damping is introduced to stabilize the system. If the virtual damping is too large, the damper feedback can introduce perceptible noise. Therefore, design becomes a three-way trade-off between stability, noise rejection, and accuracy.

Adding delay to spring and spring-damper displays reduces effective damping by $K(T/2 + t_d)$. Similarly, adding delay reduces effective mass for damper displays by $B(T/2 + t_d)$. This result demonstrates that intentionally adding delay could offset device damping or mass, however, adding delay can introduce non-passive effective jerk feedback that feels unnatural, and also has the potential to drive the system unstable.

Colgate and Shenkel established that a haptic display is guaranteed stable when coupled to passive, but other arbitrary, human impedance if, and only if, it is passive [6]. A haptic display is passive if its closed-loop transfer function is positive real [14], which implies that the Bode plot of the system impedance has phase inbetween -90° and 90° at all frequencies, or equivalently, the effective damping is positive at all frequencies. For frequencies where the haptic display has non-positive effective damping, the haptic display is capable of producing energy.

The theoretical and experimental analyses show that time delay strongly affects rendered and characterized damping, but does not have a significant affect on effective or characterized stiffness. In other words, the *actual* stiffness of the haptic display does not significantly change with time delay. For the human user studies, we observed that the effect of time delay on *perceived* damping and stiffness was well predicted by the *characterized* results: time delay affects perceived damping, but not perceived stiffness. This result can be contrasted with the perceived stiffness results of Ishihara and Negishi, Knorlein et al., and Luca et al. [17],

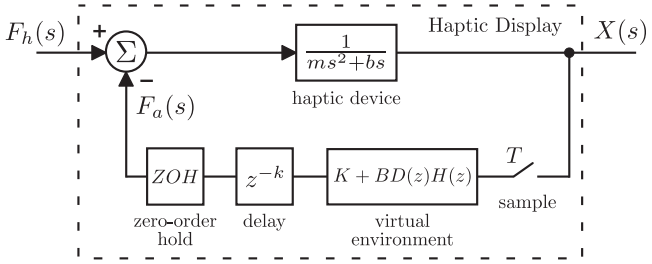

Fig. 9. Block diagram for a haptic display modeling sampling, a discrete-time control law, and the zero-order hold.

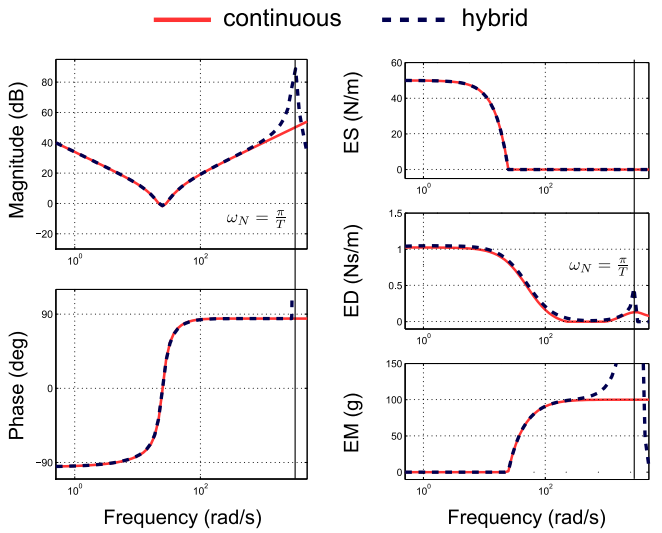

Fig. 10. Closed-loop impedances of the entirely continuous and hybrid system models. The impedances are similar for frequencies below the Nyquist frequency, $\omega_N = \pi/T$.

[18], [22], that reported that perceived stiffness *decreased* with time delay, and the results of Pressman et al. [27], that reported that perceived stiffness *increased* with time delay. The discrepancy between experiments can be explained by human perception of stiffness depending on more factors than the actual mechanical properties of the display, such as semantic ambiguity, visual information [9], and the nature of the interaction [26], [28]. Understanding the relationship between the infinite dimensional *rendered* dynamics and the human *perceived* dynamics is central to designing accurate haptic displays. By establishing how the rendered mechanical properties of the display change with time delay, it is possible to isolate and study the effect of other factors which influence human perception, and is an area for future work.

Many models could be used to describe a haptic display rendering a virtual environment; our choice of the model shown in Fig. 1 was driven by relevance as a practical design tool, tractability for finding solutions using conventional linear control theory, and our ideas about the most significant factors in system accuracy. In future work, we may examine additional system properties, such as modeling actuator dynamics and backlash.

8 Conclusion

Our results presented how closed-loop rendered impedances are affected by key parameters for haptic displays with spring, damper, and spring-damper virtual environments. We established that spring and spring-damper haptic displays render the desired effective stiffness only up to the frequency defined by Equation (4). Damper and spring-damper haptic displays render the desired effective damping up to the cut-off frequency of the low-pass filter. We showed that a system impedance can be characterized by a mass, damper, spring impedance optimally by the solution to a convex optimization problem. The fidelity of the model is provided by the Average Distortion Error. We presented an analysis showing that time delay has no significant effect on rendered and characterized stiffness, and reduces rendered and characterized damping by the product of virtual stiffness and total time delay. Reducing the low-pass filter cut-off frequency reduces the rendered damping bandwidth, and the characterized damping. The rendered and theoretical dynamics analyses were validated with experimental data gathered with a Phantom Premium 1.5. The perceived dynamics were investigated using human user experiments. Similar to the rendered and characterized dynamics, we observed no significant effect of time delay on perceived stiffness, and increasing time delay resulted in reduced perceived damping. Lower filter cut-off frequencies resulted in lower perceived damping. The contribution of this work facilitates the design of haptic displays by providing a theoretical framework for how system parameters affect closed-loop impedance.

Appendix
Comparison of Continuous and Hybrid Model

We performed our analysis using an entirely continuous model of the haptic display. However, in reality, the control of a physical haptic device is performed through a computer containing A/D (analog to digital) and D/A (digital to analog) components. In this section, we compare the closed-loop impedances of an entirely continuous model and hybrid (meaning containing both continuous-time and discrete-time elements) model.

A block diagram of the hybrid system model is shown in Fig. 9. The hybrid model differs from the entirely continuous system model shown in Fig. 1b by modeling the sampling and zero-order order explicitly, and by considering a discrete-time haptic control law and time delay instead of their continuous counterparts. We consider a virtual spring and damper virtual environment. To obtain an estimate of the velocity of the device, the sampled position measurements go through a discrete back differencing operator,

$$D(z) = \frac{(z-1)}{Tz}, \tag{22}$$

and then a first-order discrete low-pass filter,

$$H(z) = \frac{(1-e^{-\omega_0 T})z}{z-e^{-\omega_0 T}}, \tag{23}$$

where ω_0 (rad/s) represents the cut-off frequency of the low-pass filter. The continuous delay element is replaced by a discrete one,

$$e^{-t_d s} \rightarrow \frac{1}{z^k}, \tag{24}$$

where k is a nonnegative integer.

We analyze the closed-loop impedance of the hybrid system by finding an entirely discrete model with the same input-output properties of the hybrid system. The entirely discrete system is formed by converting the zero-order hold, haptic device, and sample elements to their zero-order hold equivalent [10],

The closed-loop impedances of the entirely continuous model and hybrid system model are compared in Fig. 10. For frequencies below the Nyquist frequency ($\omega_N = \frac{\pi}{T}$ rad/s), the impedances of the two systems are very similar, but for frequencies past the Nyquist frequency, the impedances deviate substantially. Most haptic systems feature fast sampling ($T < 0.001$ s), so the results of the analysis using the entirely continuous model apply straightforwardly to a hybrid system model.

Acknowledgments

The authors thank Sean M. Sketch for his help in generating the preliminary analysis. This work was supported in part by US National Science Foundation grant 1217635.

References

[1] J. J. Abbott and A. M. Okamura, "Effects of position quantization and sampling rate on virtual-wall passivity," *IEEE Trans. Robot.*, vol. 21, no. 5, pp. 952–964, Oct. 2005.

[2] S. Boyd and L. Vandenberghe, *Convex Optimization*. New York, NY, USA: Cambridge Univ. Press, 2004.

[3] M. Cavusoglu, D. Feygin, and F. Tendick, "A critical study of the mechanical and electrical properties of the phantom haptic interface and improvements for high performance control," *Presence*, vol, 11, pp. 555–568, 2002.

[4] G. A. V. Christiansson and F. C. T. Van Der Helm, "The low-stiffness teleoperator slave – a trade-off between stability and performance," *Int. J. Robot. Res.*, vol. 26, no. 3, pp. 287–299, 2007.

[5] J. E. Colgate and J. M. Brown, "Factors affecting the z-width of a haptic display," in *Proc. IEEE Int. Conf. Robot Autom*, 1994, pp. 3205–3210.

[6] J. E. Colgate and G. G. Schenkel, "Passivity of a class of sampled-data systems: Application to haptic interfaces," *J. Robot. Syst.*, vol. 14, no. 1, pp. 37–47, 1997.

[7] N. Colonnese, S. M. Sketch, and A. M. Okamura, "Closed-loop stiffness and damping accuracy of Impedance-type haptic displays," in Proc. *IEEE Haptics Symp.*, Feb. 2014, pp. 97–102.

[8] N. Diolaiti, G. Niemeyer, F. Barbagli, and J. K. Salisbury, "Stability of haptic rendering: Discretization, quantization, time delay, and coulomb effects," *IEEE Trans Robot.*, vol. 22, no. 2, pp. 256–268, Apr. 2006.

[9] M. O. Ernst and M. Banks, "Humans integrate visual and haptic information in a statistically optimal fashion," *Nature*, vol. 415, no. 6870, pp. 429–433, 2002.

[10] G. F. Franklin, D. J. Powell, and A. Emami-Naeini, *Feedback Control of Dynamic Systems*, 4th Ed. Upper Saddle River, NJ, USA: Prentice-Hall, 2001.

[11] G. A. Gescheider, *Psychophysics: The Fundamentals*, 3rd ed. Lawrence Erlbaum, Mahwah, NJ, 1997.

[12] J. Gil, T. Hulin, C. Preusche, E. Sánchez, and G. Hirzinger, "Stability boundary for haptic rendering: Influence of damping and delay," *J. Comput. Inf. Sci. Eng.*, vol. 9, no. 1, pp. 1–8, 2009.

[13] M. Grant and S. Boyd. (2012). CVX: Matlab software for disciplined convex programming. [Online]. Available: http://cvxr.com/cvx

[14] P. G. Griffiths, R. B. Gillespie, and J. S. Freudenberg, "A fundamental tradeoff between performance and sensitivity within haptic rendering," *IEEE Trans. Robot.*, vol. 24, no. 3, pp. 537–548, Jun. 2008.

[15] N. Gurari, J. Wheeler, A. Shelton, and A. Okamura, "Discrimination of springs with vision, proprioception, and artificial skin stretch cues," in *Proc. Int. Conf. Haptics: Perception, Devices, Mobility, Commun.*, 2012, pp. 160–172.

[16] S. Hirche, A. Bauer, and M. Buss, "Transparency of haptic telepresence systems with constant time delay," in *Proc. IEEE Conf. Control Appl.*, 2005, pp. 328–33.

[17] M. Ishihara and N. Negishi, "Effect of feedback force delays on the operation of haptic displays," *IEEJ Trans. Elect. Electron. Eng.*, vol. 3, no. 1, pp. 151–153, Jan. 2008.

[18] B. Knorlein, M. Di Luca, and M. Harders, "Influence of visual and haptic delays on stiffness perception in augmented reality," in *Proc. IEEE Int. Symp. Mixed Augmented Reality*, 2009, pp. 49–52.

[19] D. Lawrence, "Stability and transparency in bilateral teleoperation," *IEEE Trans. Robot. Autom*, vol. 9, no. 5, pp. 624–637, Oct. 1993.

[20] D. Lawrence, L. Y. Pao, M. A. Salada, and A. M. Dougherty, "Quantitative experimental analysis of transparency and stability in haptic interfaces," *Haptic Interfaces Virtual Environ. Teleoperator Syst.*, vol. 58, pp. 441–449, 1996.

[21] L. Ljung, *System Identification: Theory for the User*. Upper Saddle River, NJ, USA: Prentice-Hall, 1999.

[22] M. D. Luca, B. Knorlein, M. Ernst, and M. Harders, "Effects of visualhaptic asynchronies and loadingunloading movements on compliance perception," *Brain Res. Bull.*, vol. 85, no. 5, pp. 245–259, 2011.

[23] S. McJunkin, M. O'Malley, and J. Speich, "Transparency of a phantom premium haptic interface for active and passive human interaction, in *Proc. Am. Control Conf.*, 2005, vol. 5, pp. 3060–3065.

[24] J. Mehling, J. Colgate, and M. Peshkin, "Increasing the impedance range of a haptic display by adding electrical damping," in *Proc. Eurohaptics Conf.*, 2005, pp. 257–262.

[25] L. L. Nicholson, R. D. Adams, and C. G. Maher, "Manual discrimination capability when only viscosity is varied in viscoelastic stiffness stimuli," *J. Manipulative Physiol. Therapeutics*, vol. 26, no. 6, pp. 365–373, 2003.

[26] I. Nisky, P. Baraduc, and A. Karniel, "Proximodistal gradient in the perception of delayed stiffness," *J. Neurophysiol.*, vol. 103, no. 6, pp. 3017–3026, 2010.

[27] A. Pressman, L. J. Welty, A. Karniel, and F. A. Mussa-Ivaldi, "Perception of delayed stiffness," *Int. J. Robot. Res.*, vol. 26, no. (11-12), pp. 1191–1203, 2007.

[28] M. Rank, Z. Shi, and S. Hirche, "Perception of delay in haptic telepresence systems," *Presence*, vol. 19, no. 5, pp. 389–399, 2010.

[29] G. Strang, *Linear Algebra and Its Applications*. Pacific Grove, CA, USA: Brooks/Cole, 1988.

Nick Colonnese received the BS degree from the University of Washington, Seattle, WA, in 2010, and the MS degree from Stanford University, Stanford, CA, in 2012, both in mechanical engineering. He is currently working toward the doctoral degree in the Department of Mechanical Engineering, Stanford University, Stanford, CA. His research interests include the stability and fidelity of haptic displays and bilateral teleoperation. He is supported by the Stanford Graduate Research Fellowship. He is a student member of the IEEE.

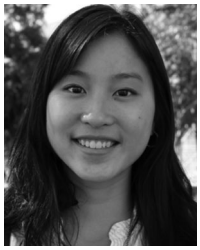

Alexa F. Siu received the BS degree in the Department of Biomedical Engineering with a minor in computer science focused on intelligence at the Georgia Institute of Technology. Starting in Autumn 2015, she will be a graduate student in mechanical engineering at Stanford University. She is a student member of the IEEE.

Caroline M. Abbott received the BS degree in mechanical engineering from Stanford University, Stanford, CA in 2014. She is currently working toward the MS degree at Stanford University, Stanford, CA, also in mechanical engineering. Her MS program focuses on fluid mechanics and energy systems. She is a member of Tau Beta Pi. She is a student member of the IEEE.

Allison M. Okamura received the BS degree from the University of California, Berkeley, in 1994, and the MS and PhD degrees from Stanford University, Stanford, CA, in 1996 and 2000, respectively, all in mechanical engineering. She is currently an associate professor of mechanical engineering at Stanford University, where she is also the Robert Bosch faculty scholar. Her research interests include haptics, teleoperation, medical robotics, virtual environments and simulation, rehabilitation, prosthetics, and engineering education. She is a fellow of the IEEE.